Low-Cost Calibrated Microwave Radiometers for Solar Observation: From Education to Science

Giacomo Schiavolini[1], Giulio Brancali[1], Ethan Bernardini[1], Giulia Orecchini[1], Valentina Palazzi[1], Camille C. A. Westerhof[2], Timo S. Prinz[2], Martin Hübner[2], Sebastian Lange[2], Maurizio Burla[2], and Federico Alimenti[1(✉)]

[1] Dipartmento d'Ingegneria, Università degli Studi di Perugia, via G. Duranti 93, 06125 Perugia, Italy
federico.alimenti@unipg.it

[2] Technische Universität Berlin, Fachgebiet Hochfrequenztechnik-Photonik Einsteinufer 25, 10587 Berlin, Germany
burla@tu-berlin.de

Abstract. Low-cost microwave radiometers can be built using a low-noise downconverter for satellite TV reception and a software-defined radio. Errors due to system gain and noise temperature drift can be corrected using motorized black body and noise injection. Successful solar observations have been made with such a radiometer mounted on a 75 cm offset parabolic dish. A joint educational project between the University of Perugia and the Technical University of Berlin is launched on this topic to give students the opportunity to practice with microwave systems, antennas, electronics and data processing.

Keywords: Microwave radiometers · electronic noise · solar observation

1 Introduction

The observation of the Sun in the microwave and mm-wave bands is a very active research field because, at these frequencies, it is possible to investigate complex physical mechanisms that characterize our star. Since the use of large radio telescopes is not always possible (the Sun is a very intense source), and the working time of these instruments is distributed among different experiments, researchers have decided to equip themselves with smaller instruments specifically designed for solar observations. In particular 2.5-m radio telescopes working up to 100 GHz have recently been proposed [9].

In this context, it would be desirable to complement the scientific data with solar brightness temperature measurements obtained with full-disk radiometers, i.e. instruments without imaging capability [21]. A network of these radiometers, distributed around the world, is needed to provide a time-on-target measurement

M. Valle et al. (Eds.): SIE 2024, LNEE 1263, pp. 142–159, 2025.
https://doi.org/10.1007/978-3-031-71518-1_17

24 h a day, 365 days a year. Consequently, the ideal instrument should be simple and inexpensive so that it can be easily replicated. The apparatus should be equipped with a calibration circuit and, possibly, with two channels at different frequencies to determine the spectral index. The design and the first experimental validation of a radiometer with these features is described in the present study.

This paper introduces the basics of radio astronomy, microwave radiometry and related electronics, as well as the use of software defined radios as instrument backend units, which is quite novel. Indeed, in the last decade, SDRs have been integrated with microwave radiometers to improve reconfigurability [15] and miniaturization, which are important issues in small satellites [6], Cubesats [14] and unmanned aircraft systems [5].

To demonstrate the feasibility of the idea, one of the less expensive SDR devices available on the market (i.e., an 8-bit SDR belonging to the RTL family) is chosen as a case study and experimentally characterized. This SDR has a software programmable gain between 20 and 50 dB, a noise figure of 7.5 dB at 1 GHz and a dynamic range of about 40 dB. The radio can be tuned between 64 and 1766 MHz with a signal bandwidth up to 3.2 MHz, performances that allow its use as an intermediate frequency receiver in radiometric applications.

2 The Students Project

A joint educational project between the University of Perugia and the Technical University of Berlin is launched to give students the opportunity to engage in the hands-on task of building an amateur radio telescope. The educational goal is to learn the basics of microwave radiometry, microwave electronics, antennas, the nature of emission and motion of astronomical objects, and to solve mechanical problems such as antenna construction, mounting and tracking. Many amateur radio astronomical projects have been proposed, and their descriptions are available in great detail in a number of books or web sites. However, not many of the described approaches offer the possibility to obtain calibrated measurement data. Instead, the ambition of this specific project is to realize a calibrated instrument, i.e. able to measure the brightness temperature of the observed celestial bodies, mainly the Sun and the Moon.

The present paper is written for the benefit of readers who want to start similar activities and, especially, is dedicated to the students involved in the project.

3 Theory

Celestial bodies such as the Sun, the Moon and radio sources emit electromagnetic radiation. These hot objects radiate like black bodies, and produce a white-noise spectrum at microwave and millimeter-wave frequencies. The Sun and the Moon, in particular, are quite strong radio astronomical sources, so they can be easily detected even with small radio telescopes. Purpose of this section is to

recall the theoretical basis that allows, under some simplifying assumptions, to predict the noise level picked up by the radio telescope antenna.

3.1 Antenna Noise Temperature

The antenna noise temperature is the physical quantity measured by microwave radiometers. Such a temperature depends on the scene observed by the antenna and can be evaluated according to [7, p. 144] as:

$$T_A = \frac{A_e}{\lambda^2} \iint P_n(\rho, \varphi)\, T_B^{obs}(\rho, \varphi)\, d\Omega \tag{1}$$

where λ is the signal wavelength, A_e is the effective area of the antenna, P_n is the normalized (power) radiation pattern, and T_B^{obs} is the brightness temperature of the observed radio source. The variables ρ and φ are used to describe the spatial variations of the above functions. In the case of a celestial body such as the Sun or Moon, it is particularly convenient to define ρ as the angular coordinate along the radius of the celestial body, and φ as the angular coordinate around the axis between the antenna and the celestial body. In the case of the Sun, this spherical coordinate system is shown in Fig. 1.

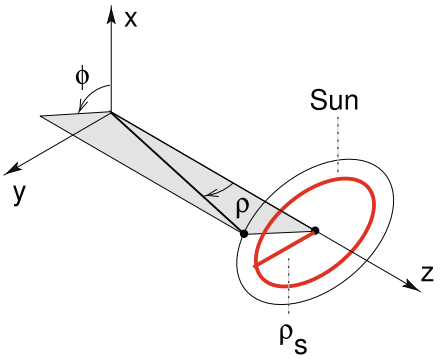

Fig. 1. Spherical coordinate system used to define the brightness temperature distribution over the solar disk (or a celestial body). The antenna is pointed at the center of the Sun. The solar radius ρ_S is equal to about 16 arcmin. The solid angle of the Sun Ω_s is defined as the cone of angular aperture ρ_S.

The antenna soild angle Ω_A is defined as:

$$\Omega_A = \iint P_n(\rho, \varphi)\, d\Omega \tag{2}$$

with the elementary solid angle $d\,\Omega$ given (in spherical coordinates) by:

$$d\,\Omega = \sin\rho\, d\rho\, d\varphi \simeq \rho\, d\rho\, d\varphi \tag{3}$$

The small-angle approximation is well verified for all celestial bodies since $\rho \leq \rho_S \ll 1$ (for the Sun $\rho_S \simeq 16\,\text{arcmin}$ which is 4.65×10^{-3} radians). It is worth noting here that the antenna theorem relates the antenna solid angle, the effective area and the wavelength squared, [10], [7, p. 144]:

$$\frac{A_e}{\lambda^2} = \frac{1}{\Omega_A} \tag{4}$$

Finally it is observed that, for most practical cases (dish antennas), Ω_A can be related to the half-power beamwidth (HPBW) $2\rho_H$ as follows:

$$\Omega_A = \kappa\,\pi\,\rho_H^2 \tag{5}$$

κ being a constant of the antenna. Note that the HPBW is twice ρ_H.

From now on we will limit our discussion to the Sun, but the same formulation applies without modification to all celestial bodies. In order to evaluate the above integral in Eq. (1), some assumptions are necessary. First, the brightness temperature of the Sun is assumed to be uniform over the solar disk:

$$T_B^{sun}(\rho,\varphi) = \begin{cases} T_S & 0 \leq \rho \leq \rho_S \\ 0 & \text{elsewhere} \end{cases} \tag{6}$$

where T_S is the average brightness temperature of the Sun. Second, since the measurements are made from Earth, both the atmospheric transmittance (τ_a) and the radio temperature of the sky (T_{sky}) must be taken into account to model the observed object:

$$T_B^{obs}(\rho,\varphi) = \tau_a\,T_B^{sun}(\rho,\varphi) + T_{sky} \tag{7}$$

At this point it is interesting to note that if the half-power beamwidth of the antenna is greater than the diameter of the Sun, the Sun can be assimilated to a point-like source (assuming the antenna is pointed at the center of the Sun), while the sky is an extended source. This is the case for inexpensive microwave radiometers with small antennas. Furthermore, we observe that τ_a and T_{sky} depend on the antenna elevation above ground, although this is not explicitly stated in (7). Inserting (7), (6) into (1) and using (4) one gets:

$$T_A = \frac{\tau_a}{\Omega_A} \iint_{\Omega_s} P_n(\rho,\varphi)\,T_B^{sun}(\rho,\varphi)\,d\Omega \;+\; T_{sky}\,\underbrace{\frac{1}{\Omega_A}\iint d\Omega}_{1} \tag{8}$$

An estimate of the antenna noise temperature can thus be obtained by evaluating the first integral over the solid angle of the Sun Ω_s:

$$T_A \simeq \frac{\tau_a}{\Omega_A} \int_0^{2\,\pi} d\varphi \int_0^{\rho_S} T_S\,\underbrace{P_n(\rho,\varphi)}_{\approx 1}\,\rho\,d\rho + T_{sky} \tag{9}$$

where $P_n(\rho, \varphi) \simeq 1$ since this study assumes an antenna with $\Omega_A \gg \Omega_s$. As previously said we are considering small antennas whose beam is much larger than the solar radius (full disk radiometers). Performing the above calculations:

$$T_A \simeq \tau_a \frac{\pi \rho_S^2}{\Omega_A} T_S + T_{sky} = \frac{\tau_a}{\kappa} \frac{\rho_S^2}{\rho_H^2} T_S + T_{sky} \tag{10}$$

where (5) is finally used to express Ω_A in terms of the half-power beamwidth. In the above relationship the term ρ_S^2/ρ_H^2 is known as the filling factor and justifies the dilution of T_S across the antenna beam.

The previous formulation assumes an ideal antenna with unit efficiency, i.e. with $\eta_A = 1$. Substituting η_A in (10), we get the effective antenna noise temperature T_A', i.e. the quantity that is measured by the microwave radiometer:

$$T_A' = \eta_A T_A + (1 - \eta_A) T_{amb} \tag{11}$$

In this equation, T_{amb} is the ambient temperature. The last term represents the thermal noise generation associated with the antenna ohmic losses. The final result is obtained by combining (10) and (11):

$$T_A' \simeq \eta_A \frac{\tau_a}{\kappa} \frac{\rho_S^2}{\rho_H^2} T_S + \underbrace{T_{sky} + (1 - \eta_A) T_{amb}}_{T_{sky}'} \tag{12}$$

with T_{sky}' being the apparent sky temperature. In the following of the paper it will be shown that the apparent temperature can be easily determined from measurements, and that it can be used to estimate the antenna efficiency.

3.2 Gaussian Antennas

Aperture antennas used in radio astronomy can often be approximated as Gaussian beam focusing elements. Using such an approximation it is possible to estimate the antenna solid angle and thus the parameter κ. According to [7, p. 136] the normalized radiation pattern of a gaussian beam focusing element is:

$$P_n(\rho) = \exp\left(-2 \frac{\rho^2}{\rho_0^2}\right) \tag{13}$$

where ρ_0 is the far-field divergence angle and the Gaussian beam radiation pattern, being axially symmetric, is a function of the angle ρ only. Evaluation of Ω_A with (2) gives:

$$\Omega_A = \pi \frac{\rho_0^2}{2} \tag{14}$$

The relationship between ρ_0 and ρ_H (half-power angle) is obtained from (13):

$$\rho_0 = \sqrt{\frac{2}{\ln 2}} \rho_H \tag{15}$$

and, as a result, we can express Ω_A in terms of ρ_H:

$$\Omega_A = \pi \underbrace{\frac{1}{\ln 2}}_{\kappa} \rho_H^2 \tag{16}$$

In conclusion, comparing (5) with (16) we have found that, for a Gaussian beam, $\kappa = 1/\ln 2 \simeq 1.443$.

3.3 Brightness Temperature of the Quiet Sun

The brightness temperature of the quiet Sun averaged over the whole solar disk has been studied by many radio astronomers in the last decades, [12,21]. In particular the following empirical relationship (based on more than three decades of observations) is reported in [12]:

$$\log(T_S) = a + b \log(f_0) \tag{17}$$

where log is the base 10 logarithm, f_0 is the observation frequency in Hz, and the constants $a = 6.43$ and $b = -0.236$ represent the 1-Hz temperature extrapolation and the spectral index respectively. The above linear fit (in log scale) is valid in the range 10–100 GHz. In our case the observation frequency is 12.6 GHz and a quiet Sun brightness temperature $T_S \simeq 11000\,\mathrm{K}$ is calculated.

4 Material and Methods

As seen in the previous section, the microwave noise emitted from the Sun is captured by the radio telescope and produces a certain noisy signal at the antenna output. Such a noise can be accounted for assigning the effective noise temperature T'_A to the radiation resistance of the antenna, and is measured by a microwave radiometer. As a consequence, from the radiometer's point of view, the antenna appears as a matched resistor that emitting thermal noise at an equivalent physical temperature T'_A. A total power radiometer consists of a microwave receiver followed by a true rms power detector. Since the input noise level is very low, a significant amount of gain should be provided by the receiver to make the output signal compatible with the power detector range. Assuming a perfect power matching between the antenna and the receiver, the available noise power N_o at the detector input (or at the front-end output) is given by:

$$N_o = k_B\,(T'_A + T_{rx})\,B_{rx}\,G_{rx} \tag{18}$$

where G_{rx}, T_{rx}, and B_{rx} are the available receiver power gain, equivalent noise temperature, and bandwidth, respectively, and $k_B = 1.38^{-23}\mathrm{J/K}$ is the Boltzmann constant. In a superheterodyne architecture, B_{rx} is determined by the IF filter. The inverse (18) is the basic (total power) radiometer equation:

$$T'_A = \underbrace{\frac{1}{k_B\,B_{rx}\,G_{rx}}}_{\alpha} N_o - \underbrace{T_{rx}}_{\beta} = \alpha\,N_o - \beta \tag{19}$$

Such an equation states that there is a linear relationship between the measured output noise power N_o and the antenna noise temperature T'_A. The radiometer scale factor α and the offset β should ideally be constants determined by some a priori calibration. In practice, this is not true because receiver gain and noise temperature can change significantly as a function of the physical temperature of the receiver electronics. The drifts of α and β are the main source of systematic errors, and to correct them a periodic calibration of the radiometer is necessary. In general, since two instrument parameters are unknown, two independent measurements are required. This is usually done by pointing the antenna toward two black bodies of known physical temperatures $T_{bb}^{(1)}$, $T_{bb}^{(2)}$ and using (19) to set a linear system of equations:

$$\begin{cases} N_o^{(1)}\,\alpha - \beta = T_{bb}^{(1)} \\ N_o^{(2)}\,\alpha - \beta = T_{bb}^{(2)} \end{cases} \tag{20}$$

which can be solved for α and β. This approach requires some instrument engineering (e.g., a movable black body), which will be discussed below, along with other calibration methods (noise injection).

Another methodological aspect to consider is that N_o results from the measurement of a noisy signal. This leads to the fluctuation of its value and thus to the fluctuation of the estimate of T'_A. The standard deviation of such a quantity is known as the radiometer resolution ΔT and represents the minimum temperature variation that can be measured by the instrument. Hersman and Poe [8] demonstrated the following relationship for a total power radiometer:

$$\Delta T = (T'_A + T_{rx})\,\sqrt{\frac{1}{\tau\, B_{rx}} + \left(\frac{\Delta G}{G_{rx}}\right)^2} \tag{21}$$

where τ is the integration time, while the $\Delta G/G_{rx}$ term accounts for the total receiver gain drift and fluctuations that occur during the integration time. A low standard deviation ΔT thus implies maximizing the $\tau\, B_{rx}$ product and minimizing the $\Delta G/G_{rx}$ gain fluctuations.

Figure 2 shows the microwave radiometer architecture considered in this study. The system is based on satellite TV low noise frontend [16]. An input signal in the 11.6–12.70 GHz band is converted to an IF signal between 0.95 and 2.05 GHz. These devices have a typical gain of 54 dB with a noise figure of less than 0.8 dB. Two polarizations and different input frequency bands can be selected electronically in the more advanced units. The average price of these devices is about $20, so low-cost instruments are feasible.

The basic configuration uses an analog backend. This consists of an IF amplifier, a ceramic bandpass filter, a Schottky diode square-law power detector, an integrator, and a video amplifier. The signal is acquired by a 10-bit ADC and sent to a computer. A more advanced configuration uses a software defined radio (SDR) to perform IF amplification, bandwidth selection, and power detection. The latter is achieved by processing the sampled In-phase and Quadrature (I/Q) signal components in real time.

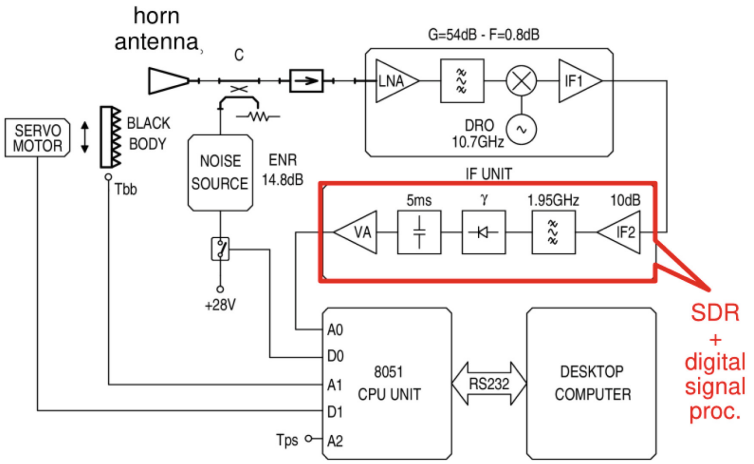

Fig. 2. Block diagram of the low-cost microwave radiometer used in the solar experiments. The classical architecture is based on analog IF amplification, detection and integration stages to process the received signal (analog backend). A software defined radio can replace the IF unit with several advantages (SDR backend).

In this paper, the SDR radiometer is proposed as the main solution. This approach is in fact quite new and offers several advantages, as described in the rest of the paper. From this point of view, we want to show that an SDR can be used to measure microwave noise with good accuracy. However, the radiometer with analog backend is a mature instrument, so it will be adopted to make a first Sun observation and to validate the model summarized by Eq. (12).

4.1 Radiometer with SDR Backend

In the previous section it has been described a novel microwave radiometer concept based on a low-noise downconverter for satellite TV reception and a software-defined radio. The latter works as an IF stage, performing amplification, filtering and power detection functions [17].

The SDR approach has many advantages. First, it simplifies the design of the instrument, since it is based on high-level components already available on the market. Second, the IF frequency can be tuned digitally within the output bandwidth of the downconverter (0.95 to 2.05 GHz), which is very important for eliminating interference from TV satellites. Finally, two channels can be processed simultaneously, allowing the spectral index to be determined. Such a parameter is of great interest to radio astronomers.

This study is based on the SDR shown in Fig. 3 (top panel). Although high-performance SDRs are now available on the market (see, for example, the Adalm Pluto family from Analog Devices), our interest is in the performance that can be achieved with low-cost devices. In particular, we focused on RTL-SDR using the Rafael R820T RF tuner and the Realtek RTL2832U demodulator [19]. The RF

interface consists of a reconfigurable integrated superheterodyne architecture. The front-end can be programmed to acquire signals between 64 and 1766 MHz with a maximum gain of 50 dB that can be set by software. A Low-Noise Amplifier (LNA) is used as the first stage and this ensures a typical noise figure of 3.5 dB at 500 MHz. The input reflection coefficient S_{11} is about -10 dB at 1000 MHz in a 50 Ω environment. The received signal is then filtered and frequency shifted before sampling and acquisition. Two 8-bit Analog-to-Digital Converters (ADCs) are used for this purpose, giving a dynamic range (with fixed RF gain) of about 40 dB. Due to the complex sampling (in-phase and quadrature signal components) it is possible to acquire the signal bandwidth up to the sampling rate. This can go up to 3.2 Mb/s and is software controlled. The ADCs and all the devices required for digital signal processing and communication via the USB interface are integrated in the Realtek RTL2832U chip.

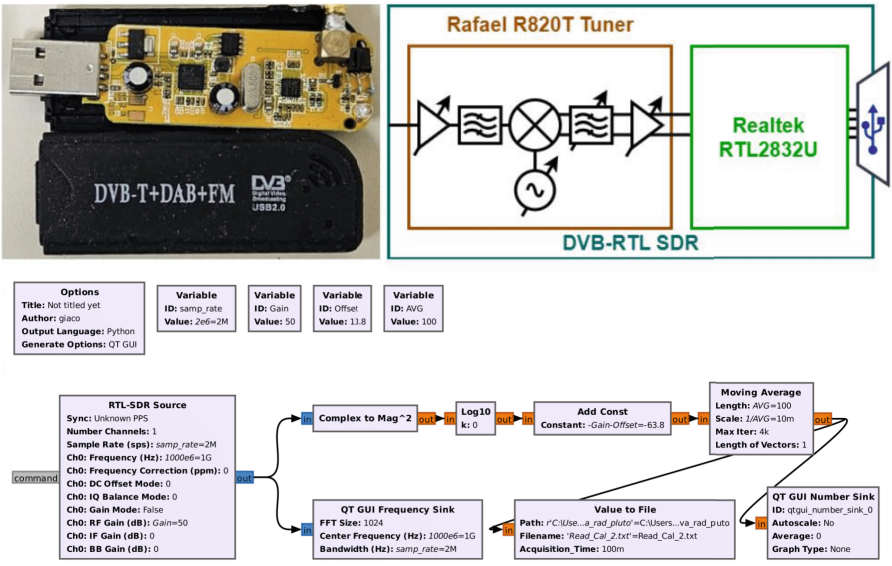

Fig. 3. RTL-SDR that can be used as radiometer backend. Hardware (top left), block diagram (top rigth) and GNURadio software (bottom).

To configure the radio and extract the desired data, a diagram-based GNU-Radio script was implemented. In this program, as a first step, we configure the SDR with the RTL-SDR source block. Then, the instantaneous power $p(\ell)$ at the SDR output is evaluated, in the discrete time domain, as the square magnitude of the complex signal. Using the in-phase $i(\ell)$ and quadrature $q(\ell)$ signal components:

$$p(\ell) = i^2(\ell) + q^2(\ell) \tag{22}$$

where ℓ is the discrete time, so the continuous time is given by $t = \ell\,\Delta t$ with sampling period Δt. Such a value is finally integrated over time, as required by

the processing of microwave radiometer data:

$$\bar{p}(\ell) = \frac{1}{L_\tau} \sum_{\ell=1}^{L_\tau - 1} p(\ell) \tag{23}$$

In this expression the integration time τ is given by $\tau = L_\tau \, \Delta t$.

To use the SDR in microwave noise measurements it is important to relate the power P_o at the SDR output with the input power P_i. This can be done with the following model:

$$P_o = G_{sdr} \, (P_i + k_B \, F_{sdr} \, T_0 \, B_{sdr}) \tag{24}$$

where G_{sdr} is the total SDR gain (which can be set by software), F_{sdr} is the SDR noise figure, and $T_0 = 290\,\mathrm{K}$ is the IEEE standard temperature for noise[1]. Observe that the SDR badnwidth B_{sdr} determines the bandwidth of the whole system (low-noise downconverter + SDR) since it is the narrow one. As a result we can assume $B_{rx} = B_{sdr}$ in Eq. (18).

4.2 Radiometer with Analog Backend

A breadboard of the microwave radiometer with analog backend is depicted in Fig. 4 (left panel). Although a complete account of such an instrument can be found in [2] and [18], a brief description of the adopted electronic circuits is also given here for the reader's convenience.

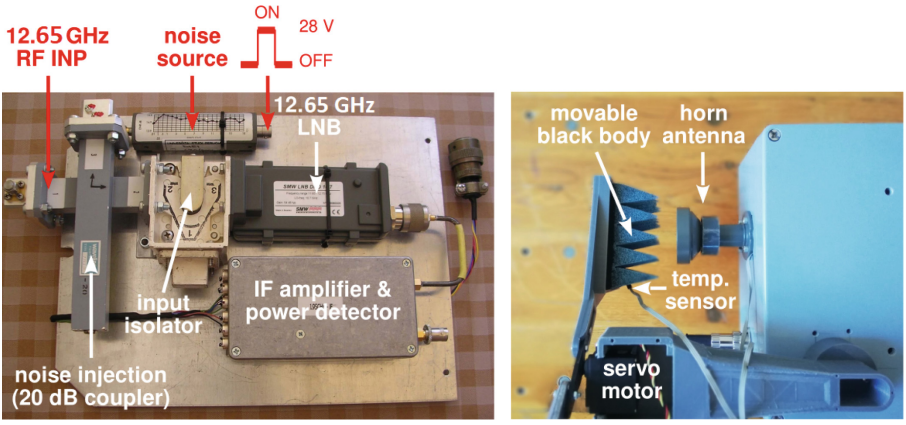

Fig. 4. Breadboard of the 12.65 GHz radiometer equipped with the analog backend.

A downconverter from Swedish Microwave was used to implement a superheterodyne receiver. The downconverter is characterized by a 0.8 dB noise figure,

[1] G_{sdr} and F_{sdr} are frequency dependent, so they should be determined (with an appropriate calibration procedure) at the frequency at which the SDR is tuned.

a 54 dB RF gain, and a gain drift with temperature of less than 0.1 dB/K. The local oscillator is an integrated 10.7 GHz dielectric resonator oscillator (DRO) with −75 dBc/Hz phase noise at 1 kHz offset from the carrier and excellent stability over temperature. Thus, an input RF signal between 11.65 GHz and 12.75 GHz is downconverted to an output IF signal between 0.95 GHz and 2.05 GHz. The image frequencies (8.65 GHz to 9.75 GHz) are rejected by more than 50 dB by a bandpass filter integrated into the downconverter. The LNB input port is a standard WR75 rectangular waveguide.

The analog IF chain is a custom design to match the characteristics of the downconverter. It consists of an input bias tee to power the downconverter, a fixed 10 dB attenuator to set a 50 Ω input impedance of the IF chain, a two-stage monolithic amplifier to provide IF gain, a digital attenuator to fine tune the system gain, and a 1.95 GHz ceramic bandpass filter to define the radiometer IF bandwidth. The filter bandwidth is 100 MHz. All of these components are integrated on a single PCB fabricated by an industrial process on 0.8 mm FR4 material. The entire IF circuit has a total gain of about 10 dB. Since the center IF frequency is 1.95 GHz, the radiometer operating frequency is set to 12.65 GHz.

The square-law power detector (true rms detector) operates at 1.95 GHz and is integrated on the same board as the IF. It is implemented with a zero bias Schottky diode (HSMS2850) together with a narrow band LC impedance matching. The obtained detector sensitivity is about 7.2 mV/μW. A 5 ms analog integrator consists of a simple passive RC filter connected to the square-law detector output. Video amplification is done with an instrumentation amplifier whose voltage gain is factory trimmed to 100.

The radiometer is fully calibrated to compensate for both gain and system noise temperature drifts. This is achieved using a movable black body and noise injection circuitry The movable black body (see right panel of Fig. 4) is used to correct for receiver noise temperature drifts, i.e. to determine the radiometric offset β. It consists of a piece of pyramidal microwave absorbing material. A servo motor periodically moves the black body in front of the horn antenna to close the horn aperture. Meanwhile, a temperature sensor measures the physical temperature of the black body. Instead, the noise injection circuit uses the MT7600 laboratory noise source from Maury Microwaves and a −20 dB Moreno coupler in the WR75 waveguide (see left panel of Fig. 4). When the bias input of the MT7600 is set to 28 V, a known amount of noise power is generated by this device and injected into the receiver input through the directional coupler. Recently, integrated avalanche noise diodes have been proposed that allow an extreme miniaturization of such a circuit [3].

With these calibration mechanisms, two equations similar to (20) can be set, and as a result, α and β can be determined. The receiver gain is updated every 3 s (noise injection), while the receiver noise temperature is corrected every 30 min. It is important to note that since there is a strong dependence of the radiometric gain on the internal physical temperature of the instrument, estimation and compensation techniques can be successfully implemented as proposed in [4].

5 Results

A proof of concept for the low-cost microwave radiometer is presented in this section. The experimental discussion is divided into two parts: first, the RTL-SDR radio is validated as a digital instrument backend. Then, the radio telescope is pointed at the Sun, the antenna noise temperature is measured, and the results are compared with the developed theory.

5.1 RTL-SDR Characterization

Since the use of the SDR as a digital backend of the microwave radiometers is quite novel, it is necessary to demonstrate the feasibility of such an approach. For this purpose, two different experiments are designed as shown in Fig. 5. In the first experiment, the RTL-SDR is connected to an RF signal generator (Rohde & Schwarz SMB100B up to 30 GHz) and the radio is tested with continuous wave (CW) signals. In the second experiment, a laboratory noise source (Keysight 346C-K01) is used instead to characterize the radio against noisy signals.

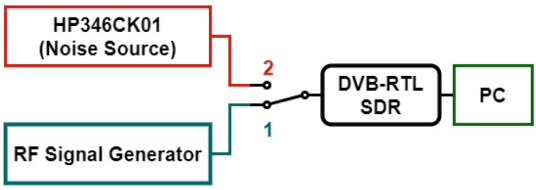

Fig. 5. Experimental setup adopted to characterize the RTL-SDR.

The CW setup is used to characterize the RTL-SDR as a function of the gain settings that are software-programmed into the device. To do this, the RF generator applies a specific carrier to the input. The available power level of the R&S SMB100B can range from −120 to 20 dBm and is therefore suitable for checking both the sensitivity and the saturation limits of the device under consideration. The I/Q signals produced by the RTL-SDR under these conditions are sampled, transferred to the PC and used to evaluate the output power with the Eqs. (22), (23). At $f_0 = 1\,\text{GHz}$, the values obtained are shown in Fig. 6 (upper panel) and clearly show that as the gain is increased, the operating range of the radio moves towards lower power levels. The dynamic range (distance between saturation and noise limits) is about 40 dB and, as mentioned before, is determined by the number of ADC bits (8 in our case). With this experiment it is also possible to determine the true gain G_{sdr} of the radio as a function of the gain settings. Using such a true gain, the input power can be retrieved from the measured output power, as shown in Fig. 6 (bottom panel). From this figure, it is clear that within the dynamic range, and almost ideal behavior is obtained.

The noise figure F_{sdr} is the second parameter used to model the RTL-SDR according to (24). The noise setup of Fig. 5 is used to experimentally determine

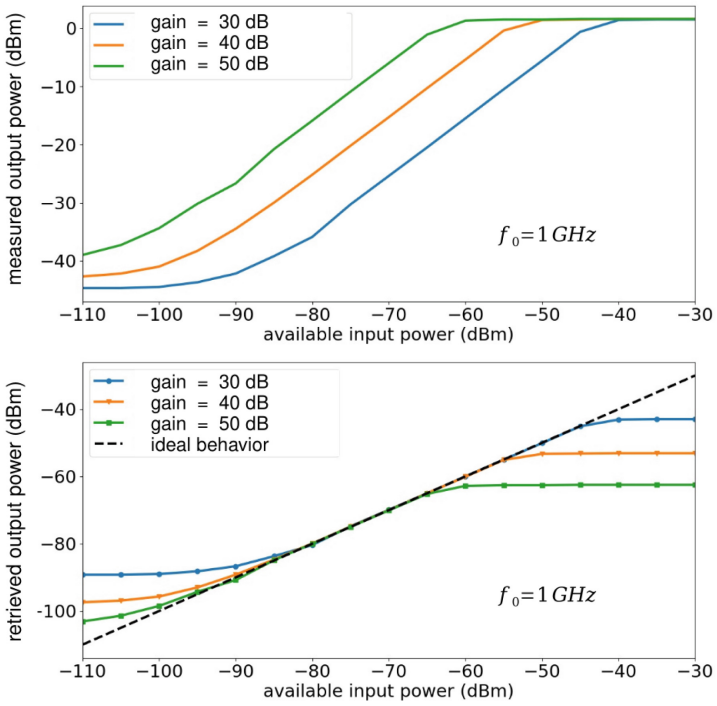

Fig. 6. Results of the RTL-SDR continuous-wave (CW) experiments. Measured output power (top) and retrieved input power (bottom) for different gain settings. This characterization is carried out at 1 GHz.

F_{sdr}. For this purpose, the Y-factor method is applied [1] and the results are shown in Fig. 7 (upper panel) as a function of the gain settings when the receiver is tuned at 1 GHz. The noise figure obtained follows the typical behavior of a receiver with variable LNA gain. When the gain of the first stage of the RF chain is increased, a general decrease in the noise figure is observed. On the other hand (see Fig. 6) the radio saturates at lower power levels. The RTL-SDR parameters determined with the above experiments are summarized in Table 1.

In a final experiment, the RTL-SDR input is connected to a matched load at ambient temperature and the input equivalent noise temperature is retrieved from the measured output power and using the previously estimated device parameters (i.e., G_{sdr} and F_{sdr}). It is seen that the radio can detect its own noise and that the fluctuations of the retrieved noise temperature (standard deviation) can be reduced by increasing the integration time τ. In a more rigorous way, the Allan deviation of the input noise temperature fluctuations are evaluated together with the corresponding confidence intervals [20]. In fact, through the correct interpretation of the Allan deviation result, a large amount of information directly related to the acquisition system performance can be extracted [11].

Table 1. RTL-SDR parameters

gain settings (dB)	G_{sdr} (dB)	F_{sdr} (dB)
30	44.3	22.3
35	49.4	18.4
40	54.4	13.1
45	58.8	10.8
50	63.6	7.0

$f_0 = 1\,\text{GHz}$, $B_{sdr} = 2\,\text{MHz}$

From the analysis performed on the RTL SDR, shown in Fig. 7, it can be seen that the acquisition starts to drift after about 100 s.

5.2 Sun Experiments

Successful Sun observations were made on October 27, 2023 with the radiometer of Fig. 4. As mentioned above, the instrument operates at 12.65 GHz and has a radiometric resolution of 1-K when observing a black body at ambient temperature. The instrument is equipped with a 70 cm off-axis parabolic antenna for satellite TV applications and is mounted on a stable base. In these experiments, the antenna is pointed in a fixed direction in the sky and the Sun passes through the beam due to the Earth's rotation. The pointing direction (azimuth and elevation angles) was predicted using astronomical software according to the radio telescope's location and the time of day.

To use the antenna temperature model summarized by Eq. (12) four parameters must be known, namely: the antenna half-power angular radius ρ_H, the antenna efficiency η_A, the atmospheric transmissivity τ_a, and the apparent sky temperature T'_{sky}. The latter can be easily determined as the measured antenna noise temperature when the Sun is completely outside the antenna beam. In our experiments we measure a value around 47 K, as shown in the figure.

The true sky temperature and the atmospheric transmissivity are a function of the elevation angle (30° in our case), the sky conditions (clear sky during the experiments), and other parameters such as temperature, pressure, and relative humidity at ground level. Very accurate remote sensing models are nowadays available to predict these parameters [13]. The October 27, 2023 was a rather hot afternoon and the external radiometer temperature sensor measured about 30 C ($T_{amb} = 303\,\text{K}$). Pressure and humidity were taken from those reported by the Perugia weather station. As a result a true sky temperature $T_{sky} = 12.7\,\text{K}$ and an atmospheric transmissivity $\tau_a = 0.96$ were estimated. Now, reversing the relationship between true and apparent sky temperature, the antenna efficiency is obtained:

$$\eta_A = 1 - \frac{T'_{sky} - T_{sky}}{T_{amb}} \tag{25}$$

As a result we get $\eta_A \simeq 0.89$, a quite interesting value.

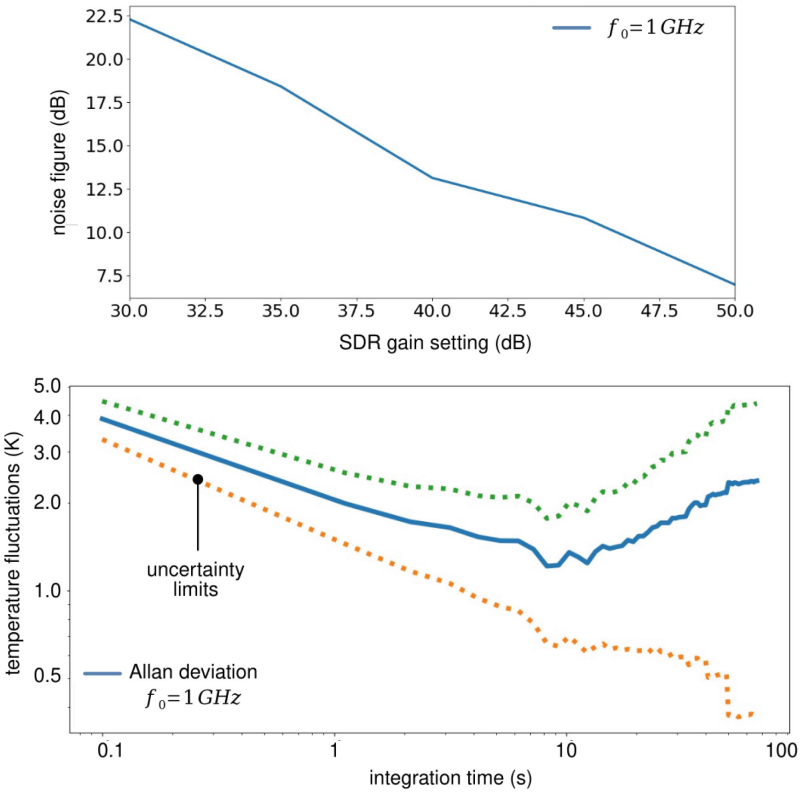

Fig. 7. Results of the RTL-SDR noise experiments. Noise figure at 1 GHz (top) and Allan deviation of the input noise temperature fluctuations (bottom). The 100 s integration time corresponds to 1000 samples at 10 Hz acquisition rate

The antenna radiation pattern with the instrument in its final configuration (parabolic dish, feed horn, structure) is determined using the Sun as the radio source and the Earth's rotation as the scanning mechanism. In particular, it is obtained from the measured antenna noise temperature by removing the sky offset and normalizing the peak of the curve to one. Finally, the acquisition time is converted into an angle using the Earth's rotation speed of 4° per minute, and this is plotted on the x-axis. The radiation pattern derived in this way is shown in the upper left panel of Fig. 4 and is well approximated by Eq. (13) with a half-power beamwidth ($2\,\rho_H$) equal to 2.2°[2] (Fig. 8).

Figure 4 (lower left panel) represents another recording experiment. A peak noise temperature of 450 K is obtained when the instrument is pointed at the

[2] In this study the solar disk is not deconvolved, i.e. the Sun is assumed to be a point source. Furthermore, due to the latitude and time of observation, the Sun passes diagonally through the antenna beam. As a result, the curve obtained does not represent a radiation pattern cut in the vertical or horizontal plane.

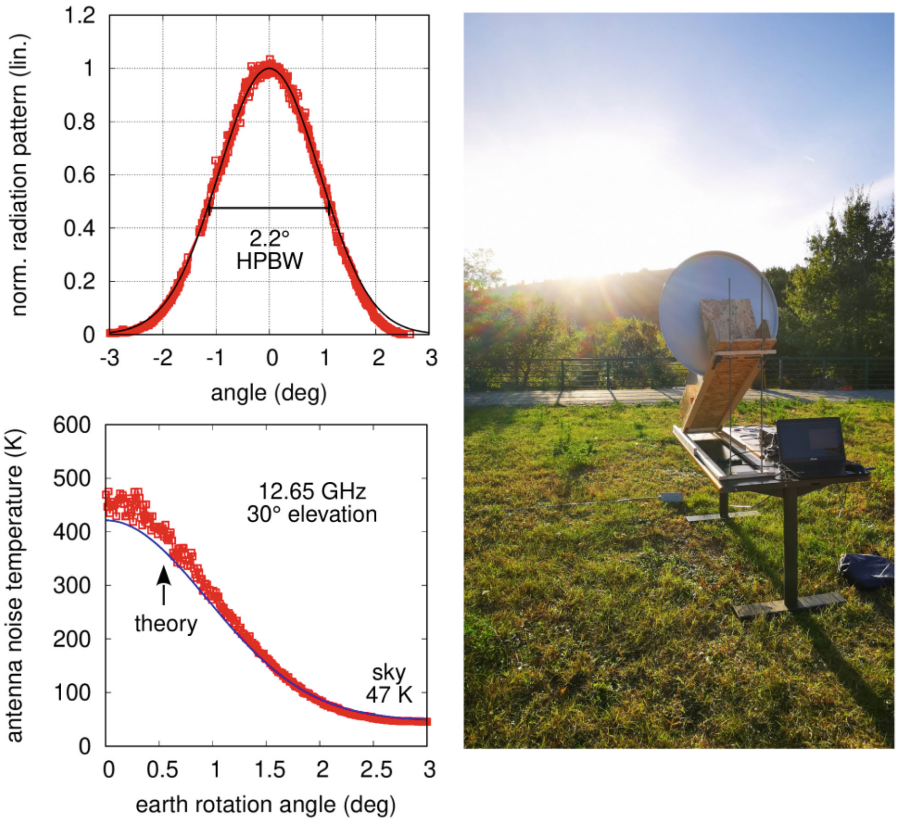

Fig. 8. Results of the October 27, 2023 experiments. The Gaussian beam approximation (13) is in good agreement with measured data (top left panel).

center of the Sun (starting point). The measurements are in good agreement with the proposed theory (system parameters previously estimated) and with solar brightness temperature models [12]. This result is very promising, as it shows that scientific quality data can be obtained with a simple and inexpensive instrument.

6 Conclusion

The breadboards of a low-cost microwave radiometer and radio telescope have been designed and successfully tested in a significant environment. The prototype instrument is capable of measuring the Sun's brightness temperature, and the experimental results are in good agreement with theoretical models.

A joint student project has been launched between the University of Perugia and the Technical University of Berlin, focusing on the construction of small radio telescopes for solar observation. The project is intended to be carried out

by students following an electronic engineering curriculum, and is an opportunity for them to practice with electronics, antennas, microwave systems, and data processing. In addition to the educational value of the project, the students will be able to approach real scientific activities and broaden their knowledge in an interdisciplinary way, particularly in the direction of physics and astronomy.

Finally, based on the foundations laid by this work and as a further development of the proposed breadboards, it will be possible to conceive a miniaturized instrument suitable for flight on board Cubesats. With such an approach, solar observations and solar flare detection will be possible from a space-based platform, thus eliminating the errors associated with atmospheric transmissivity variations. To the best of the author's knowledge, such a scientific mission has never been attempted worldwide.

Acknowledgements. This work is partially supported by: the Erasmus+ programme, the Italian Ministry of University and Research (MUR) in the frame of the "PON 2022 Ricerca e Innovazione" action, the University of Perugia with the "AstroCube" project, and the European Union with the ERC "ELEPHANT" project, contract nr. 948624.

The authors wish to acknowledge Prof. Stefania Bonafoni for the computation of sky temperature and atmospheric transmissivity with the most accurate remote sensing models available in the literature.

F. Alimenti wish to acknowledge the students Simone Burchia and Keidi Kacaku, University of Perugia, for their contribution to some of the experimental results reported in the paper. M. Burla also wishes to acknowledge all the students of the 2024 SIERRA project at TU Berlin for their contributions to the first experimental implementation of an amateur radio telescope at TU Berlin.

References

1. Agilent Technologies: Application Note 57-1: Fundamental of RF and Microwave Noise Figure Measurements (2000)
2. Alimenti, F., et al.: A low-cost microwave radiometer for the detection of fire in forest environments. IEEE Trans. Geosci. Remote Sens. **46**(9), 2632–2643 (2008)
3. Alimenti, F., Tasselli, G., Botteron, C., Farine, P., Enz, C.: Avalanche microwave noise sources in commercial 90-nm CMOS technology. IEEE Trans. Microwave Theory Tech. **64**(5), 1409–1418 (2016)
4. Bonafoni, S., Alimenti, F., Roselli, L.: An efficient gain estimation in the calibration of noise-adding total power radiometers for radiometric resolution improvement. IEEE Trans. Geosci. Remote Sens. **56**(9), 5289–5298 (2018)
5. Farhad, M., Alam, A., Biswas, S., Rafi, M., Gurbuz, A., Kurum, M.: SDR-based dual polarized L-band microwave radiometer operating from small UAS. IEEE J. Sel. Top. Appl. Earth Obs. Remote Sens. **17**, 9389–9402 (2024)
6. Fernandez, L., et al.: SDR-based Lora enabled on-demand remote acquisition experiment on-board the Alainsat-1. In: IEEE International Geoscience and Remote Sensing Symposium (IGARSS), Brussels, Belgium, pp. 8111–8114 (2021)
7. Goldsmith, P.F.: Quasioptical Systems: Gaussian Beam, Quasioptical Propagation and Applications. IEEE Press (1998)
8. Hersman, M.H., Poe, G.A.: Sensitivity of the total power radiometer with periodic absolute calibration. IEEE Trans. Microwave Theory Tech. **29**(1), 32–40 (1981)

9. Italian National Institute for Astrophysics (INAF): A Smart Solar Imaging System at High Radio Frequency for Continuous Solar Monitoring and Space Weather Applications (2023). https://sites.google.com/inaf.it/solar. Accessed 21 June 2024
10. Kraus, J.D.: Radio Astronomy. McGraw-Hill, New York (1966)
11. Land, D., Levick, A., Hand, J.: The use of the Allan deviation for the measurement of the noise and drift performance of microwave radiometers. Meas. Sci. Technol. **18**, 1917–1928 (2007)
12. Landi, E.: The quiet-sun differential emission measure from radio and UV measurements. Astrophys. J. **370**, 1629–1636 (2008)
13. Mattioli, V., Basili, P., Bonafoni, S., Ciotti, P., Westwater, E.: Analysis and improvements of cloud models for propagation studies. Radio Sci. **44**, 1–13 (2009)
14. Munoz-Martin, J., Capon, L., de Azua, J.R., Camps, A.: The flexible microwave Payload-2: a SDR-based GNSS-reflectometer and L-band radiometer for Cubesats. IEEE J. Sel. Top. Appl. Earth Obs. Remote Sens. **13**, 1298–1311 (2020)
15. Nelson, M.: Implementation and evaluation of a software defined radio based radiometer. Master's thesis, Iowa State University (2016)
16. Rawle, W.D., Lonc, W.P.: A small microwave total power radiometer. IEEE Antennas Propag. Mag. **34**(2), 53–54 (1992)
17. Schiavolini, G., et al.: SDR based radio-frequency noise measurements. In: 2024 IEEE Space Hardware Radio Conference (SHaRC), San Antonio, TX, USA, pp. 27–29 (2024)
18. Tasselli, G., Alimenti, F., Bonafoni, S., Basili, P., Roselli, L.: Fire detection by microwave radiometric sensors: modeling a scenario in the presence of obstacles. IEEE Trans. Geosci. Remote Sens. **48**(1), 314–324 (2010)
19. Vachhani, K., Mallari, R.: Experimental study on wide band FM receiver using GNURadio and RTL-SDR. In: International Conference on Advances in Computing. Communications and Informatics (ICACCI), Kochi, India, pp. 1810–1814 (2015)
20. Wiegelmann, A., Drake, S., Rehman, S., Chen, S.: Cost-effective Allan deviation measurement in SDRs using integrated ADC. In: IEEE Radio and Wireless Symposium (RWS), San Antonio, TX, USA, pp. 130–133 (2024)
21. Zirin, H., Baumert, B., Hurford, G.: The microwave brightness temperature spectrum of the quiet sun. Astrophys. J. **370**, 779–783 (1991)